STRUCTURAL CONTROL AND HEALTH MONITORING
*Struct. Control Health Monit.* 2011; **18**:660–673
Published online 8 April 2010 in Wiley Online Library (wileyonlinelibrary.com). DOI: 10.1002/stc.393

# Damage analysis of reinforced concrete buildings by the acoustic emission technique

A. Carpinteri[1], G. Lacidogna[1,*,†] and G. Niccolini[2]

[1]*Department of Structural Engineering and Geotechnics, Politecnico di Torino, Corso Duca degli Abruzzi 24, 10129 Torino, Italy*
[2]*National Research Institute of Metrology–INRiM, Strada delle Cacce 91, 10135 Torino, Italy*

## SUMMARY

This paper presents a research work in which the stability of a multi-storeyed building in reinforced concrete, with two visible macrocracks periodically subjected to visual inspection, is assessed by the acoustic emission (AE) technique. The observed proportionality between the rates of recorded AE activity from the cracks and the measured crack growth rates confirms significantly the effectiveness of the AE technique for damage evolution assessment in structural elements. The AE activity has been correlated with the size of the source crack advancements by some fitting relationships established using models from Damage Mechanics, Fracture Mechanics and Geophysics. Copyright © 2010 John Wiley & Sons, Ltd.

Received 14 April 2009; Revised 24 February 2010; Accepted 25 February 2010

KEY WORDS: concrete; crack; AE technique; *b*-value; damage parameter

## INTRODUCTION

The demands for assuring the safety and the performance in Civil Engineering requires as non-invasive as possible inspections to estimate the physical conditions of in-service structures. Visual inspections are quick, convenient, inexpensive and are a necessary first step. Unfortunately, they can be used to inspect only the surface, are inspector-dependent and do not provide quantitative information. Early detection of the internal damage, instead, is crucial for making decision on maintenance and rehabilitation in civil structures, in order to assure safety and extension of their service life.

An advanced method of quantitative non-destructive evaluation of damage evolution is the AE technique. Technically, the expression 'acoustic emission' is used to mean a class of phenomena in which transient elastic waves, in the range of ultrasound usually between 20 KHz and 1 MHz, are generated by the rapid release of energy from localized sources within a material. AE waves propagate through the material towards the surface of the structural element, where they can be detected by sensors, which turn the released strain energy packages into electrical signals. In this way information about the existence and location of possible sources is obtained [1–6]. In contrast to other non-destructive testing methods, like the ultrasound method, which actively probes the structure, AE technique listens for acoustic emissions (AEs) from active defects, typically growing cracks. In general, AE sources are also

*Correspondence to: G. Lacidogna, Department of Structural Engineering and Geotechnics, Politecnico di Torino, Corso Duca degli Abruzzi 24, 10129 Torino, Italy.
†E-mail: giuseppe.lacidogna@polito.it

friction, corrosion, phase changes, debonding between fibers and matrix in composite materials, plastic deformations and magnetic processes in metals, etc. [7].

Herein the AE technique is successfully used in long-term monitoring of two macrocracks appeared in a sustaining wall of a building with a reinforced concrete structure, rising near Turin (Piedmont, North-western Italy). In this particular case, in fact, the AE technique is specifically used to detect crack growth, by attaching the AE transducers near two active macrocracks. The observed proportionality between AE and crack growth rates suggests that AE is really related to the growth of cracks, while other AE source mechanisms can be neglected.

Obviously, there are fundamental differences between the different approaches to AE measurements due to the developments in electronics and sensor technologies [8].

The AE equipment used by the authors (ATEL equipment) [3,6] is capable to perform the more traditional parameter-based analysis, where only signal parameters are recorded without storing the complete waveforms. The method of analysis used with this equipment, referred to as *events counting*, is broadly used for the identification of defects with the AE technique. Moreover, this type of equipment—in the presence of a slow crack growth, and when the load and environmental conditions are not so severe, as in the case of the monitored building—is very useful to carry out long-term monitoring, given the reduced number of data to be recorded and analyzed.

The leading-edge equipment adopted by authors (USAM equipment), suited to perform the quantitative signal-based analysis, consists of many AE units, which can be synchronized for multi-channel data processing. Each unit contains a preamplified narrowband PZT sensor. The most relevant signal characteristics (arrival time, amplitude, duration and number of oscillations) are downloaded to a PC for a multi-channel data processing. From this elaboration microcracks localization is performed and the condition of the monitored specimen can be determined [4].

Using the USAM device, a laboratory test on a fibre-reinforced concrete beam under flexural loading was also conducted. After setting an appropriate detection threshold in the AE acquisition system to filter out mechanical vibrations or the environmental noise, no spurious signals were detected before the beginning of the test (i.e. no events without cracks). During the laboratory test the AE source points were located, and the progression of AE activity in the specimen volume was thus correlated with the measured crack advancements. Also in this case, it was underlined the proportionality between AE and crack grows rates as it was done for the building.

Considering some of the fundamental articles on the AE technique cited in the references [1,2,8–10], it is possible to say that the use of the parameter-based analysis is mainly related with defect formation and failures in structural elements. The signal-based analysis is related to the study of AE waveforms, and to the change of their properties, as functions of sources and wave propagations mechanisms. Moreover, both approaches deal mainly with tests conducted in the laboratory.

The novelty of this work consisted in the application of the parameter-based analysis to a damaged civil structure under service. With this procedure, taking in to account the energetic approach from Linear Elastic Fracture Mechanics, and the statistical techniques from the Geophysics, e.g. the *b*-value of the well-known Gutenberg–Richter (GR) law, the gradual drop in the crack propagation velocity was analyzed. At the same time, it was demonstrated that the AE events counting technique permits a fast and effective *in situ* assessment of the ongoing damage phenomena in full-scale structures.

## EXPERIMENTAL INVESTIGATION

### *Structural scheme of the monitored building*

The monitored building, with a rectangular plan of $25 \times 12\,m^2$ and a total height of 22 m, has a basement and 6 storeys above ground (Figure 1(a),(b)). The architectural and structural design project was drawn up in 1961.

The structure of this building, in reinforced concrete, has columns supporting the brick-concrete slabs with built-in beams with structural depth of 20 cm. At the basement level, the



DOI: 10.1002/stc

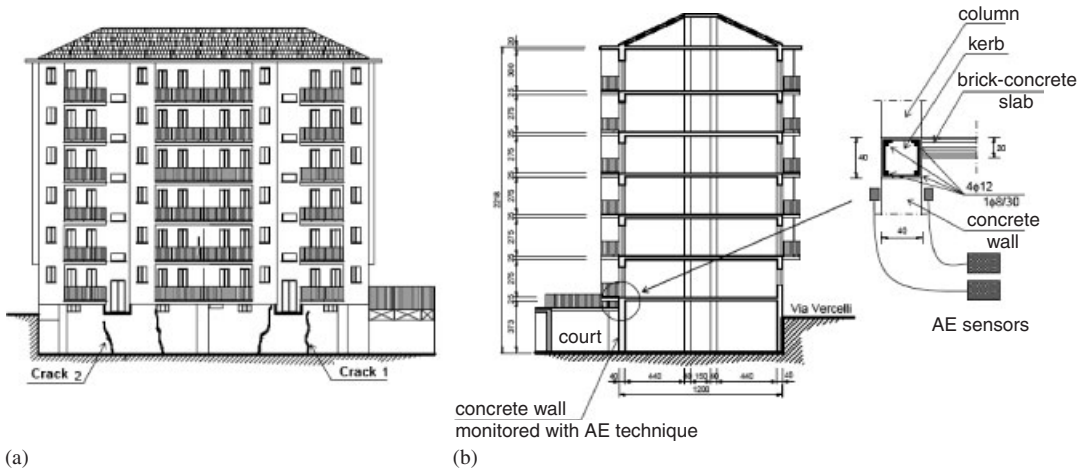


Figure 1. The monitored building: cracks in the concrete wall (a) and cross-sectional view (b).

construction is delimited on two opposite sides by supporting concrete walls, 3.73 m high and 40 cm thick, which also play as a continuous foundation for the columns of the two facades. The cross-sectional view in Figure 1(b) illustrates the structural set-up of the building, made up of three spans and eight storeys, including the attic. In this case too, there are no orthogonal beams to stiffen the structure in the crosswise direction.

*AE equipment*

The adopted equipment consisted of four AE sensors of ATEL series [3,5,6], calibrated on frequencies between 50 and 500 kHz, and four signal processing units for signal conditioning and processing, which include signal transmission, amplification, filtering and extraction of the AE signal features. A preamplifier with 40 dB gain, as an integral part of the AE sensor, converts the signal from the sensor into a suitable low-impedance signal for transmission over long distances through coax cable up to the signal processing and analysis system. The system provides additional signal amplification (60 dB), and the frequency filtering removing unwanted frequency signals, below 50 and above 500 kHz. Extraction of AE signal features, i.e. counts, is performed with a threshold measuring system, a recorder and an oscillation counter (Figure 2(a),(b)). Each processing unit was equipped with a 12 V lead battery ensuring a signal processing range of approx. 200 h.

AE sensors are piezoelectric (PZT) transducers, which exploit the capacity of certain crystals to produce electric signals whenever they are subjected to a mechanical stress. The ATEL sensors, acting as strainmeters, transform mechanical vibrations (AE) of $\sim 10^{-7}$ mm amplitude into electric signals (AE signals) of $\sim 10^{-6}$ V amplitude.

With the adopted equipment, the occurrences of AE events were simply counted. The principle of event counting is simply to count the number of times a threshold voltage $A_{\text{th}}$ (here fixed at 100 μV in order to filter out the environmental noise) is exceeded by the oscillating sensor output caused by AE activity [5,6,9,10]. Obviously, the AE transducers are sensitive to all surface vibrations lying in the frequency range between 50 and 500 kHz. This could generate a great number of received AE signals. However, due to the limits in the memory storage capacity, up to 255 counts per each period of 120 s were stored. Taking into account the typical duration of an AE signal, some tens of microsecond, the number of counts should then correspond closely to the occurred AE events (Figure 2(c)).

*Experimental results*

During the survey conducted on the building, no evident cracks were observed in either the partition walls or the curtain walls. On the other hand, four macrocracks were found in the supporting wall of concrete facing the back yard. The cracks started from the foundation of



DOI: 10.1002/stc

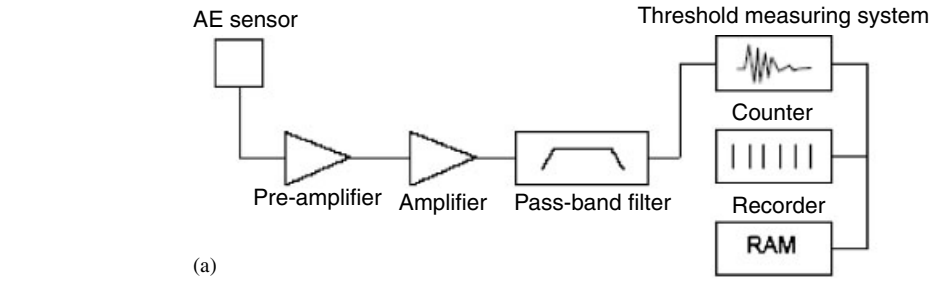


(a)

(b)

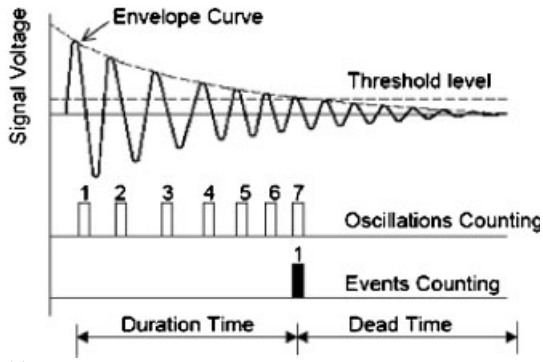


(c)

Figure 2. AE measuring system: schematic (a), and components of a single ATEL unit (b). Two counting methods applied to an AE signal (modeled by a decaying sinusoid): oscillation counting and event counting (c).

the wall and propagated through its entire thickness along the vertical direction up to the column supporting level (Figure 1(a)). The cracks width is 2 mm at the bottom of the wall and 0.2 mm at the crack tips.

The position of the reinforcement was identified by means of a pacometer, a magnetic detector that permits to determine the diameter of the reinforcing bars when the thickness of the concrete cover is known. It was ascertained that the only reinforcement in the wall is inside a kerb topping the wall, whose purpose is to distribute the concentrated loads applied by the columns. The kerb reinforcement consists of stirrups with a bar diameter of 8 mm, spaced 30 cm apart and four longitudinal bars with a diameter of 12 mm, spaced 40 cm apart in the vertical direction. Column reinforcement is appropriate for their cross-sections and the loads applied.

The ATEL AE equipment was applied near two macrocracks, shown in Figure 1(a), to determine their growth rate from the count of AE events and predict their temporal evolution. The crack growth has been monitored by both visual inspection (Figure 3) and AE technique for a time period of about 1000 h.

Comprehensive results of crack monitoring are summarized in the diagrams of Figure 4, where the accumulated crack length and AE counting number are plotted as functions of time. Proportionality between these two quantities is clear for both cracks: after partitioning the monitoring period into sub-intervals, the higher the AE counting number, the higher the crack propagation velocity.

In particular, in the proximity of the kerb reinforcement, the arrest of the cracks accompanied by saturation of the AE counting number was observed, showing in this way the reliability of AE measurements.

In such areas, in fact, the tensile stresses, which up to that point were transferred through the concrete in tension, are absorbed by the reinforcing bars so that the strength of the r.c. section is guaranteed again.

Indeed, advancement of the cracks and the associated AE activity occurred in the non-reinforced areas of the concrete wall, subjected to stresses exceeding its tensile strength, depend on the low strength of the employed material, which undergoes progressive damage.



DOI: 10.1002/stc

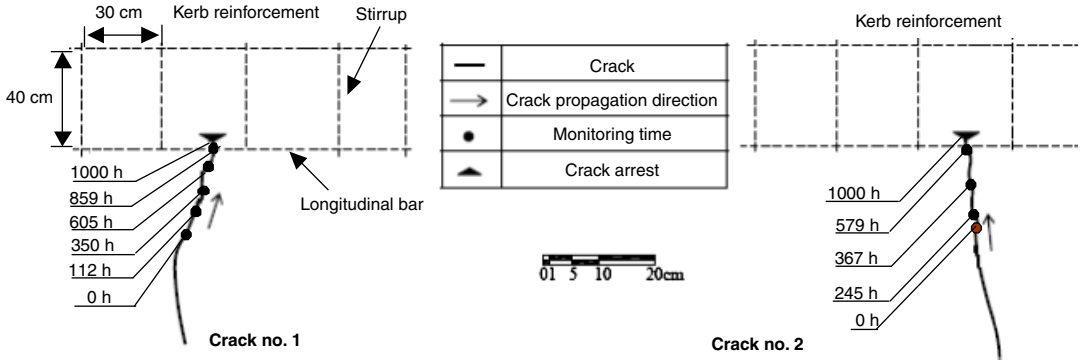


Figure 3. Results of periodical visual inspection of the two cracks.

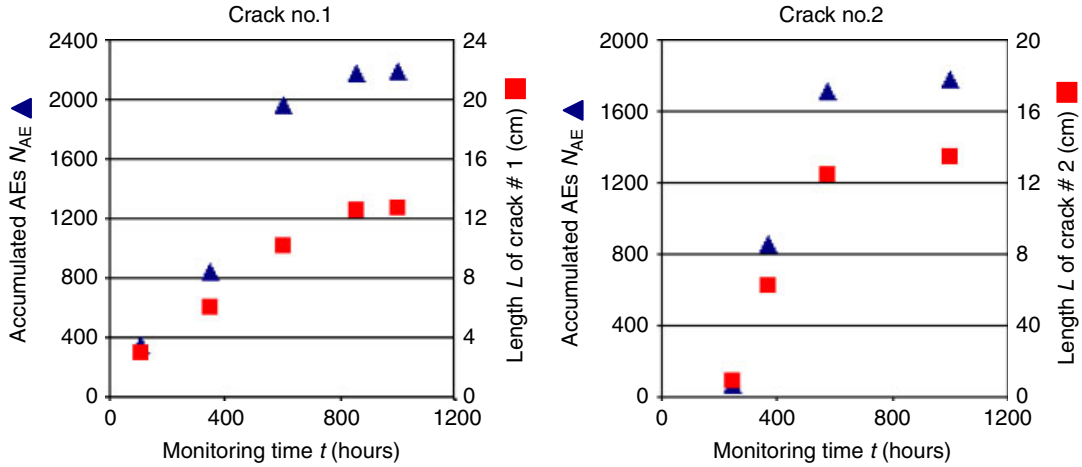


Figure 4. Dependence of the accumulated crack length (mm) and AE counting number on time for the two monitored cracks.

Table I. Experimental results obtained during the monitoring of Crack no. 1.

| Elapsed time (h) | Time window width $\Delta t$ (h) | Crack length advancement $\Delta L$ (cm) | Incremental cracked area $\Delta S/\Delta t^*$ ($CM^2/H$) | AE event counts $N$ | $b$-value |
|---|---|---|---|---|---|
| 112 | 112 | 3.0 | 1.08 | 350 | 1.69 |
| 350 | 238 | 3.0 | 0.50 | 493 | 1.78 |
| 605 | 255 | 4.1 | 0.64 | 1112 | 1.62 |
| 859 | 254 | 2.4 | 0.38 | 217 | 1.97 |
| 1000 | 141 | 0.2 | 0.05 | 20 | 2.36 |

*The incremental cracked area is estimated through the relation $\Delta S = \Delta L \cdot w$, $w = 40$ cm being the thickness of the wall.

Accordingly, strengthening interventions have been planned for this structural element, in order to stop crack propagation and restore its bearing capacity. Experimental results of crack monitoring are summarized in Tables I and II.

## APPLICATION OF THE AE TECHNIQUE

AE results from sudden energy release within a material subjected to stress or strain states. Such energy propagates through the material in the form of an acoustic wave, or AE (Figure 5(a)), which can be picked up and recorded by AE sensors applied to the surface of the structural



DOI: 10.1002/stc

Table II. Experimental results obtained during the monitoring of Crack no. 2.

| Elapsed time (h) | Time window width $\Delta t$ (h) | Crack length advancement $\Delta L$ (cm) | Incremental cracked area $\Delta S/\Delta t^*$ ($CM^2/H$) | AE event counts $N$ | $b$-value |
|---|---|---|---|---|---|
| 245 | 245 | 0.9 | 0.14 | 67 | 2.22 |
| 368 | 122 | 5.3 | 1.73 | 789 | 1.53 |
| 578 | 212 | 6.3 | 1.2 | 855 | 1.63 |
| 1000 | 421 | 1.0 | 0.09 | 66 | 2.34 |

*The incremental cracked area is estimated through the relation $\Delta S = \Delta L \cdot w$, $w = 40$ cm being the thickness of the wall.

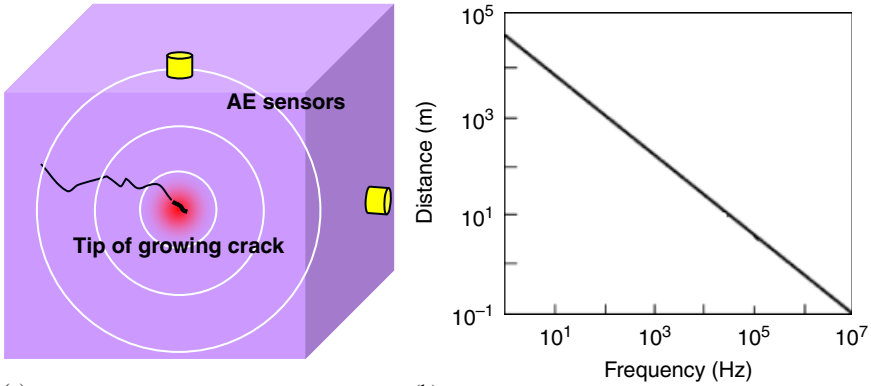


Figure 5. AE generated by a growing crack (a). Detection distance vs frequency diagram (b) (Ohtsu [2]).

elements. The mechanism is similar to that of an earthquake, but at a much smaller scale. Four AE sensors were applied to each crack, two inside and two outside the building, with their barycentres at a distance of about 3 cm from the crack tips (AE sources) in order to minimize the attenuation with distance of AE waves. Heterogeneities present in concrete can behave as diffracting elements or reflecting surfaces relatively to the propagation of AEs, causing an attenuation that limits the operating range of sensors considerably: higher-frequency components of AE waves propagate in concrete with greater attenuation, so they have a smaller detection distance [2].

In the present research work as said in Section 'AE equipment', ATEL sensors were used, and calibrated in the frequency range between 50 and 500 kHz in order to filter out disturbance signals coming from the environment: after setting an appropriate detection threshold in the AE acquisition system, it was verified that no signals due to human activities or environmental vibrations (background noise) were detected before the beginning of the monitoring. Moreover, as shown in Figure 5(b), AE signals coming from 10 m distance or more consists only of frequency components below 100 kHz, so they have only a small influence on the signals coming from the two monitored cracks [2].

*Energy-balance approach to AE*

Here, the results of the crack monitoring are interpreted by considering the energy terms involved in an AE source process: in other words, it follows the Griffith approach to Fracture Mechanics, in which now the AE term is explicitly indicated.

The considered material, in which a given amount of crack growth takes place, is part of a structural element that is under stress due to externally applied forces. There will be a certain amount of stored elastic energy when the crack growth starts, and a different amount when it stops.

This change can be expressed by (1):

$$E_a = E_b + W - \Delta E, \tag{1}$$



DOI: 10.1002/stc

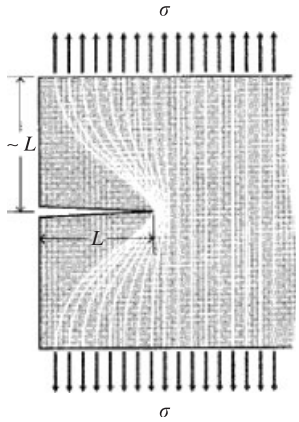


Figure 6. Idealization of unloaded region near crack flanks (Roylance [10]).

where $E_a$ is the stored elastic energy after the system has regained equilibrium, $E_b$ is the stored elastic energy before the stress, $W$ is any work done by the external forces during the crack growth, and $\Delta E$ is essentially a balancing term. When the crack has grown into a solid to a length $L$, a region of material adjacent to the free surfaces is unloaded, and a certain amount $\Delta E$ of energy is made available from the elastic field.

A simple way of visualising $\Delta E$, illustrated in Figure 6, is to regard two regions adjacent to the crack flanks, of width $L$ and height $\sim L$, as being completely unloaded, while the full stress $\sigma$ is redistributed to the remaining material [11].

This model was applied to the two monitored cracks, where $L$ is the sum of the crack increments measured during the survey. Since these cracks propagated through the entire thickness $s = 40$ cm of the wall, the total energy $\Delta E$ made available by a crack growth of length $L$ (and constant depth $s$) is then given by the elastic energy per unit volume times the volume in both regions [11,12]:

$$\Delta E = \frac{\sigma^2}{2E} \pi \, s \, L^2 \propto L^2, \tag{2}$$

where plane stress condition and linear elastic material ($\sigma = E\varepsilon$) are assumed.

The energy $\Delta E$ is the sum of different energy terms. The first term is the surface energy $E_S$ required to create new free surfaces within the material during the crack growth. The second one is the energy $E_P$ used in plastic deformation of the material. Griffith developed the concept that a pre-existing crack can propagate when the elastic energy released during the crack growth is equal to or higher than the surface energy required to create the newly formed crack surfaces. Also including plastic deformations, when $\Delta E$ is greater than the total energy ($E_S+E_P$) consumed during the crack growth, there is a surplus energy $E_{\mathrm{AE}}$ that is released in the form of AE.

These three energy terms are indicated in (3):

$$\Delta E = E_S+E_P+E_{\mathrm{AE}} \tag{3}$$

Relation (3) highlights the fact that the AE is a variable fraction of the total energy released by the crack growth.

For a given amount of crack growth, it is possible that $\Delta E$ is hardly greater than ($E_S+E_P$). In this case the deformation takes place slowly (quasi-equilibrium conditions) and there is little or no AE. On the other hand, if $\Delta E$ is substantially greater than ($E_S+E_P$), then the source event takes place rapidly and there is substantial AE [13].

Although most features of the original AE signals are sacrificed, it is possible to assume a linear scaling between the AE energy $E_{\mathrm{AE}}(t)$ and the number $N_{\mathrm{AE}}(t)$ of AEs accumulated up to time $t$ [13]:

$$E_{\mathrm{AE}}(t) \propto N_{\mathrm{AE}}(t) \tag{4}$$



DOI: 10.1002/stc

$E_{AE}(t)$ has also been correlated with the sum $L(t)$ of the crack length increments accumulated up to time $t$ by means of the relation:

$$E_{AE}(t) \propto L(t)^D, \tag{5}$$

where $D$ is an experimental fractal exponent to be determined by fitting procedures, and the AE energy is given in cumulative AE count units $N_{AE}(t)$, according to (4).

The evolution of the two cracks is estimated by comparing the growth of $\Delta E$ and $E_{AE}$ with $L$. Fitting the experimental data with (5), the dependence of $E_{AE}$ on $L$ is $E_{AE} = k\ L^D$, with similar values for the fractal exponent, $D = 1.31$ and $D = 1.22$ shown in Figure 7, revealing similar growth rate exhibited by the two cracks, while (2) establishes that $\Delta E = k'\ L^2$ ($k$ and $k'$ are proportionality constants).

Therefore, the ratio of the AE released energy $E_{AE}$ to the total energy $\Delta E$ made available by the crack growth:

$$\frac{E_{AE}}{\Delta E} = \frac{k}{k\prime}\frac{1}{L^{2-D}} \quad \text{with } 2 - D = 0.7 - 0.8 \tag{6}$$

decreases as $L$ increases, indicating a decay of the AE activity and then an evolution of the cracking process towards a stable condition.

*Damage assessment by means of the 'b-value' analysis*

The considerations reported in the previous section require cracks that are accessible to visual inspection. A more general method of damage assessment, applicable even to internal defects, is the statistical analysis of the AE signal magnitudes (the magnitude $m$ is defined through the relation $m = \mathrm{Log}(A/1\ \mu V)$, where $A$ is the peak amplitude of the signal measured in μV), which are distributed according to the GR law, the most important *empirical* law describing the scaling in fracture systems, originally introduced for earthquakes [14] and subsequently applied to the AEs [15–20]:

$$\dot{N}(\geqslant m) = \dot{a}10^{-bm}, \tag{7}$$

where $\dot{N}$ is the number of AE events per unit time with magnitude $\geqslant m$.

The exponent $b$ of the GR law, the so-called $b$-value, changes with the different stages of damage growth: dominant microcracking generates a large number of low-magnitude AE signals, while the appearance of macrocracks also generates higher-magnitude signals. That implies a progressive decrease of the $b$-value as the specimen approaches impending failure, and represents the core of the so-called '$b$-value analysis' used for damage assessment [2,4,6,15–20].

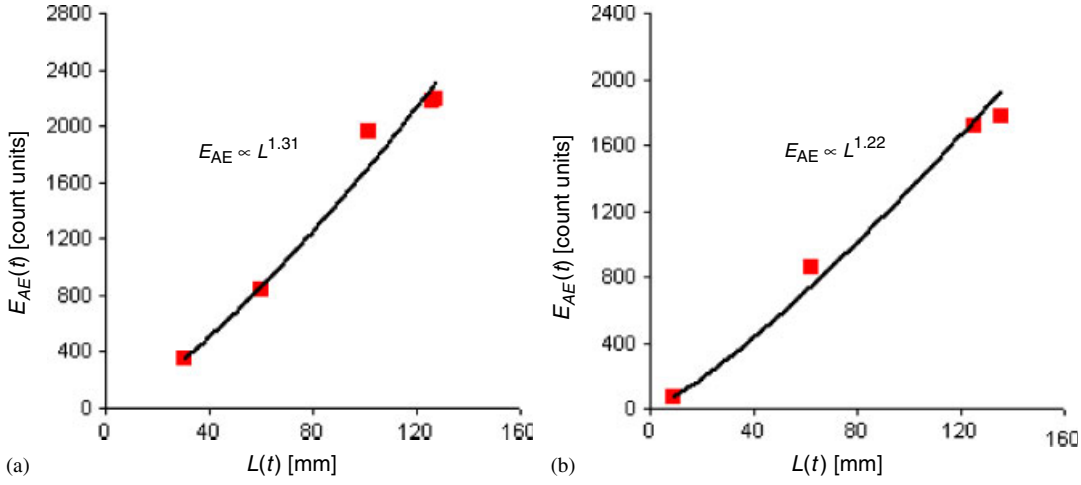


Figure 7. Accumulated AE energy $E_{AE}(t)$ vs total crack length $L(t)$ plot: (a) crack no. 1 and (b) crack no. 2.



DOI: 10.1002/stc

By calculating the logarithm of the AE signal amplitude, the mentioned *b*-value analysis allows to investigate the length distribution of a population of active cracks, exploiting the relationship between the amplitude of an AE event and the length of the source crack [17–19]. But this method is not always applicable since it requires equipments able to extract the peak amplitude from the AE signals.

Since the adopted AE ATEL equipment provides only AE event counts, a recently proposed method for estimating the *b*-value, based on the event counting technique [6,15], was used. The estimation of the *b*-value is obtained by formally applying the GR law (7) to the number of AE events counted in a specified time window, instead of the frequency–magnitude distribution. A detailed derivation of this formula is reported in [15]:

$$b = \frac{\mathrm{Log}(\dot{N}_{\mathrm{MAX}}/\dot{N})}{\mathrm{Log}\, A_{\mathrm{th}}}, \tag{8}$$

where $\dot{N}_{\mathrm{MAX}}$ is the maximum number of AE events that can be counted in a given time window, and $\dot{N}$ is the real number of event counts. Each signal exceeding a threshold voltage $A_{\mathrm{th}}$ (properly chosen in order to filter out noise) is considered as an AE event. Low *b*-values correspond to high values of $\dot{N}$, indicating a large amount of AE activity, i.e. an increased rate of damage growth, whereas high *b*-values correspond to low values of $\dot{N}$, indicating a small amount of AE activity, i.e. slow damage growth.

When AE ATEL equipment is adopted [6,15], where $A_{\mathrm{th}} = 100\,\mu\mathrm{V}$, and the counting capacity is $\dot{N}_{\mathrm{MAX}} = d \times 255$ in a time window of $T = d \times 120\,\mathrm{s}$, the *b*-value is given by:

$$b = \frac{\mathrm{Log}(d\ 255/\dot{N})}{2}, \tag{9}$$

where $\dot{N}$ is the number of ring-downs counted during the time $T$.

The observed evolution towards stability of the propagating cracks, until stopping when the cracks converged towards tougher zones of the concrete wall, is well described also by the transition from low *b*-values to higher *b*-values, calculated with (8) and illustrated in Figure 8 for both cracks.

### *Crack propagation velocity vs b-value*

The previous section has been concluded observing that low *b*-values correspond to an accelerated rate in the damage accumulation, as already reported in the AE literature [17], where a damage parameter $\eta$ has been compared with the trend of the *b*-value in AE tests on concrete beams. It has been observed that the minimum of the *b*-value corresponds to the sudden increase in $\eta$, used to describe the accumulated state of damage in the beam [17]. In this section the relationship between the *b*-value and the damage parameter $\eta$ is investigated.

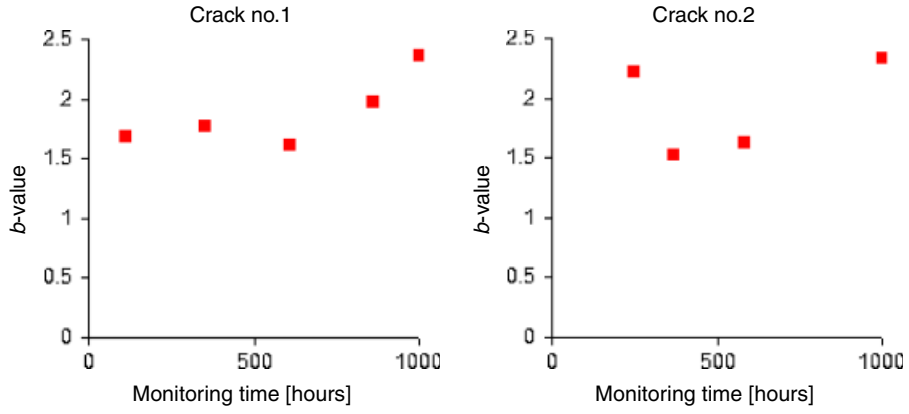


Figure 8. Temporal evolution of the *b*-value for the two monitored cracks.



DOI: 10.1002/stc

It is defined in Damage Mechanics as the normalized sum $S$ of all existing crack areas $s_i$ [12,21,22] in the material:

$$\eta(t) \equiv \frac{S(t)}{S_{\mathrm{TOT}}} = \frac{\sum_{i=1}^{N(t)} s_i}{S_{\mathrm{TOT}}}, \tag{10}$$

where $S_{\mathrm{TOT}}$ is the total crack area accumulated up to failure time $t_f$, so that $\eta(t_f) = 1$, and $N(t)$ is the number of cracks considered up to time $t$.

The presence of cracks results in a degradation of macroscopic mechanical properties of the material, such as the decrease in Young's modulus [12,21,22]:

$$\sigma = E_0(1 - \eta)\varepsilon, \tag{11}$$

where $E_0$ is the Young's modulus of the undamaged material.

The damage parameter $\eta$ is accessible to AE analysis exploiting the proportionality between the magnitude $m$ of an AE signal and the logarithm of the area $s$ of its source crack advancement [15,17,23]:

$$m \propto \mathrm{Log}\, s \tag{12}$$

from which we have [15,17,23]:

$$\eta(t) \propto \sum_{i=1}^{N(t)} 10^{m_i} \tag{13}$$

Furthermore, inserting (12) into (7), the frequency vs crack size distribution is obtained:

$$\dot{N}(\geqslant s) = \dot{c}\, s^{-b}, \tag{14}$$

where $\dot{N}(\geqslant s)$ is the number of crack advancements per unit time with an area greater than $s$.

Now, it is possible to establish an analytical relation between $\eta$, or equivalently $S$, and the $b$-value. Differentiation of (14) gives:

$$\mathrm{d}\dot{N} = \dot{c}\, s^{-b-1}\mathrm{d}s \tag{15}$$

Therefore, the total area $\dot{S}$ of cracks opened per unit time is given by:

$$\dot{S} \equiv \frac{\Delta S}{\Delta t} = \int_{s_{\min}}^{s_{\mathrm{MAX}}} s\mathrm{d}\dot{N} = \dot{c}\int_{s_{\min}}^{s_{\mathrm{MAX}}} s s^{-b-1}\mathrm{d}s = \frac{\dot{c}}{b-1}\left(\frac{1}{s_{\min}^{b-1}} - \frac{1}{s_{\mathrm{MAX}}^{b-1}}\right) \tag{16}$$

Relation (16) has been obtained in analogy with the fragmentation theories that correlate the total surface of a fragmented body with the length distribution of the fragments [24]. In [24] $s_{\min}$ and $s_{\mathrm{MAX}}$ (denoted by $r_{\min}$ and $r_{\mathrm{MAX}}$) represent respectively the size of the smallest and the largest fragment, while in this paper they represent the minimum and the maximum crack advancement.

In practice, $\Delta t$ should be short, in order to describe accurately temporal variations of the $b$-value during the crack monitoring, but also long enough to provide statistically significant $b$-value. Since a good estimate of the $b$-value requires at least 50 AE events [17–19], the width of $\Delta t$ varies as a function of the AE event rate, e.g. decreasing when the failure is imminent and the event rate increases.

The velocities of the measured crack advancements are correlated with the computed $b$-values by means of the fitting curve defined in (16), and shown in Figure 9. The fitting parameters, $s_{\min}$ and $s_{\mathrm{MAX}}$, obtained by the least square method optimization procedure, are similar for cracks 1 and 2 (see again the caption of Figure 9), confirming similar crack dynamics. As expected, the higher the damage growth rate $\dot{S}$, the smaller the $b$-value. Better spread of data point (particularly suitable for crack 1) could be obtained improving the statistics, i.e. considering more experimental points.

Looking at (16), the upper limit $s_{\mathrm{MAX}}$ for the area of crack advancements is generally controlled by the size of the cracking structural element, while the lower limit $s_{\min}$ is likely to be controlled by the scale of the heterogeneities involved in cracking, for example, the grain size.



DOI: 10.1002/stc

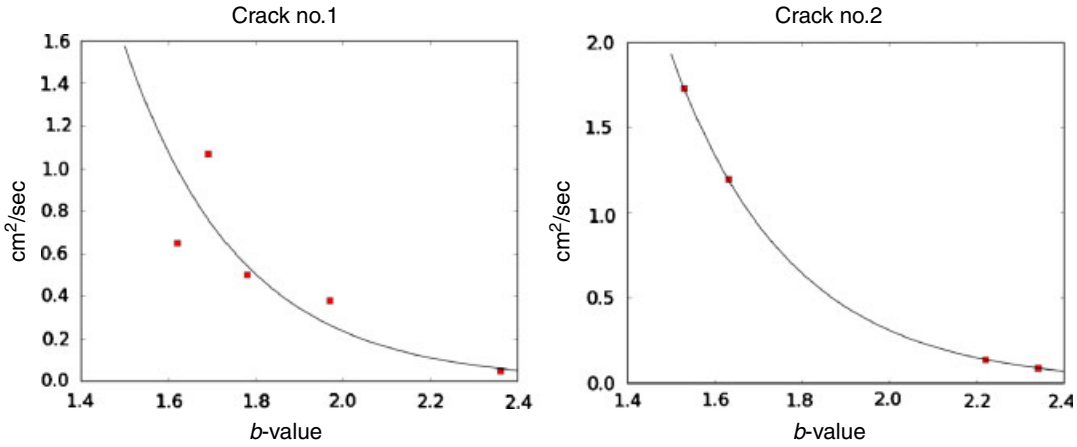


Figure 9. $\dot{S}$ vs $b$-value diagram for the monitored cracks: experimental points and fitting curve given by (16).

If $b>1$, it is necessary to specify $s_{\min}$ but not $s_{MAX}$ in order to obtain a finite crack propagation velocity $\dot{S}$:

$$\dot{S} \cong \frac{C}{b-1}\frac{1}{s_{\min}^{b-1}} \tag{17}$$

In other words, at low damage levels (high $b$-values), the crack propagation velocity is dominated by the scale of the heterogeneities.

If $b<1$, instead, it is necessary to specify $s_{MAX}$ and not $s_{\min}$:

$$\dot{S} \cong \frac{C}{1-b}\frac{1}{s_{MAX}^{b-1}} \tag{18}$$

Therefore, when the damage level is high (low $b$-values), the crack propagation velocity $\dot{S}$ is likely to be controlled by the size of the structure.

*Three-point bending test*

Finally, a sophisticated analysis on the AE data from a fiber-reinforced concrete (FRC) beam loaded up to failure was perfomed. The test was conducted in normal laboratory room conditions, at a temperature of $20\pm1^{\circ}$C, and $42\pm4\%$ relative humidity, according to the three-point bending test geometry. The beam, $1000\times150\times150\,mm^3$, had a fiber content of $40\,kg/m^3$ for a resulting Young's modulus of 35 Gpa, and a central 50 mm notch to ensure the development of a central crack during the test, performed with constant displacement rate of $10^{-}3$ mm/s (Figure 10(a)) [25–27].

As said in the Introduction, an array of USAM PZT transducers was used. These transducers, resonant in the range of 50–800 kHz, are designed with the detection of fracture precursors, i.e. high-frequency AE, in mind.

After setting an appropriate detection threshold in the AE acquisition system, it was verified that no signals were detected before the beginning of the test (i.e. no events without cracks). From each signal the arrival time was recorded, determined with an accuracy of about 0.5 μs, and the amplitude, i.e. the peak voltage of the signal itself. Although a calibration diagram fulfilling metrological requirements of the adopted PZT transducers has yet to be determined, the electrical signal can be assumed to be proportional to the acceleration at the specimen surface over the considered bandwidth, and thus be used to quantify signal amplitude.

Six transducers were applied to the specimen at the points shown in Figure 10(a),(b). The AE source location procedure allowed to identify the fracture process zone developed during the loading test. In this way, AE clusters were seen to propagate with increasing load, following satisfactorily the growth of the central crack (see Figure 10(a)) [25–27].



DOI: 10.1002/stc

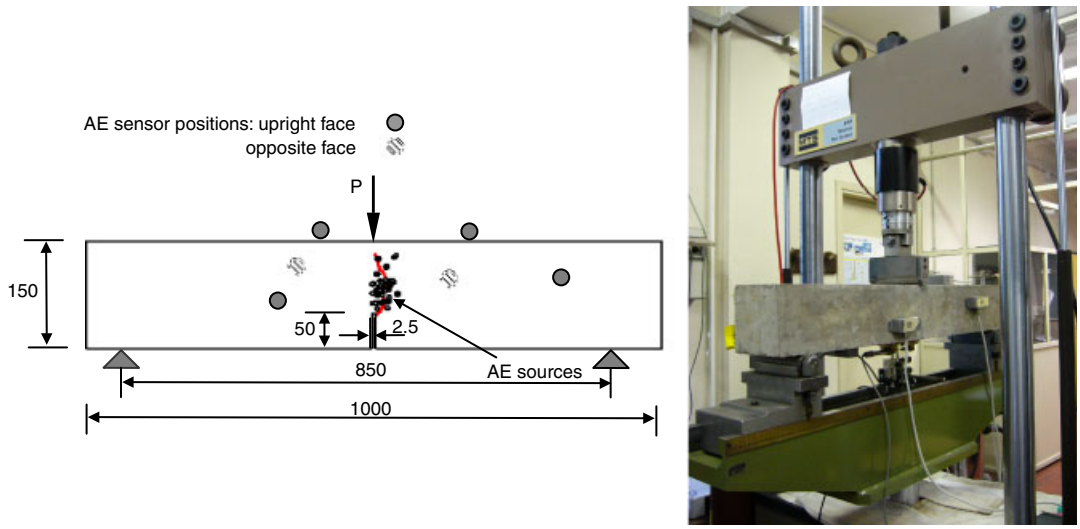


(a) (b)

Figure 10. Three-point bending test geometry, sensor positions and identification of the fracture by the localized AE sources (black points) (a). Test rig and instrumented beam in the laboratory (b).

Table III. Experimental results obtained during the monitoring of the main crack observed during the three-point bending test.

| Time window width $\Delta t$ (s) | Crack length advancement $\Delta L$ (cm) | Incremental cracked area $\Delta S/\Delta t^*$ ($CM^2/S$) | $b$-value |
|---|---|---|---|
| 875 | 4.4 | 0.040229 | 1.11 |
| 700 | 2.2 | 0.025143 | 1.31 |
| 475 | 1.0 | 0.016842 | 1.49 |
| 525 | 0.7 | 0.010667 | 1.71 |

*The incremental cracked area is estimated through the relation $\Delta S = \Delta L \cdot w$, $w = 8$ cm being the thickness of the beam.

Calculating the logarithm of the AE signal amplitude for each time window (see Table III), the measured velocities of the crack advancements were measured, and then correlated with the computed $b$-values by means of the fitting curve defined in (18), and shown in Figure 11.

In conclusion, through the mentioned distinction between low and high damage levels, the relation (16) makes it possible some interesting considerations about the connections between the crack propagation rate and the $b$-value, providing important information on the criticality of the damage process.

## CONCLUSIONS

Coupling visual inspections with AE monitoring of external macrocracks, the damage evolution in a sustaining wall of a multi-storey building, and in a fiber-reinforced concrete beam, under three-point bending test, was successfully analyzed. It was also shown that, the AE event counting technique permits a fast and effective *in situ* assessment of ongoing damage phenomena in full-scale structures.

For the multi-storey building, the visual inspections show that the monitored cracks grew until they reached zones that are able to withstand the tensile forces involved (i.e. zones such as the concrete kerb that are equipped with metal reinforcement), yielding the final crack arrest. Gradual drop in the crack propagation velocity is faithfully reproduced by the trend of the AE data, analyzed in three different ways: the event counting, the $b$-value analysis and an energetic approach coming from Linear Elastic Fracture Mechanics. Furthermore, a relationship between



DOI: 10.1002/stc

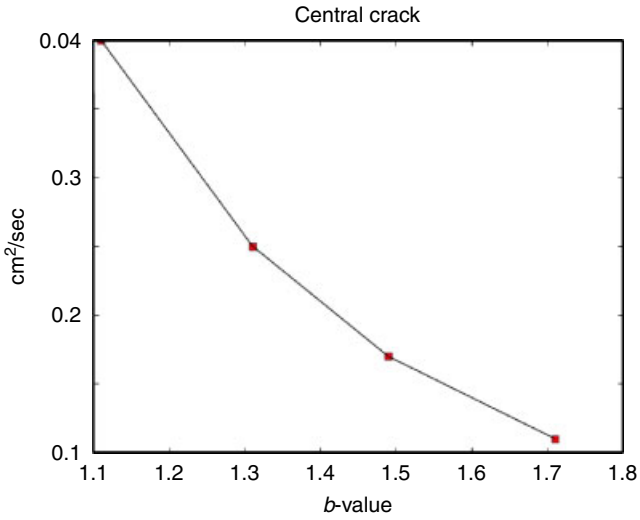


Figure 11. $\dot{S}$ vs $b$-value diagram for the main crack observed during the three-point bending test: experimental points and fitting curve given by (18): the fitting parameters are $s_{\min} = 2.18$ and $s_{MAX} = 77.19$.

crack propagation velocity and $b$-value has been derived, exploiting the properties of a statistical damage model.

The proposed relationship fitted quite correctly the experimental data both *in situ* and in laboratory and was shortly discussed.

## ACKNOWLEDGEMENTS

The authors express their gratitude to Architects Massimo Aprile and Luigi Bacco, for the expert support provided during this investigation, and Architect Vincenzo Antonaccio, who authorized the monitoring of the buildings. They also thank the ATEL Company of Pomezia (Rome) that supplied the AE measuring apparatus.

## REFERENCES

1. Shah SP, Li Z. Localisation of microcracking in concrete under uniaxial tension. *ACI Materials Journal* 1994; **91**:372–381.
2. Ohtsu M. The history and development of acoustic emission in concrete engineering. *Magazine of Concrete Research* 1996; **48**:321–330.
3. Carpinteri A, Lacidogna G, Pugno N. Richter's laws at the laboratory scale interpreted by acoustic emission. *Magazine of Concrete Research* 2006; **58**:619–625.
4. Carpinteri A, Lacidogna G, Niccolini G. Critical behaviour in concrete structures and damage localization by acoustic emission. *Key Engineering Materials* 2006; **312**:305–310.
5. Carpinteri A, Lacidogna G. Damage monitoring of an historical masonry building by the acoustic emission technique. *Materials and Structures* 2006; **39**:161–167.
6. Carpinteri A, Lacidogna G, Niccolini G. Acoustic emission monitoring of medieval towers considered as sensitive earthquake receptors. *Natural Hazards* 2007; **7**:251–261.
7. Holroyd T. *The Acoustic Emission and Ultrasonic Monitoring Handbook*. Coxmoor Publishing Company: Oxford, 2000.
8. Grosse CU, Finck F. Quantitative evaluation of fracture processes in concrete using signal-based acoustic emission techniques. *Cement and Concrete Composites* 2006; **28**:330–336.
9. Pollock AA. Acoustic emission-2: acoustic emission amplitudes. *Non-Destructive Testing* 1973; **6**:264–269.
10. Brindley BJ, Holt J, Palmer IG. Acoustic emission-3: the use of ring-down counting. *Non-Destructive Testing* 1973; **6**:299–306.
11. Roylance D. Introduction to fracture mechanics, available on website: http://ocw.mit.edu/NR/rdonlyres/Materials-Science-and-Engineering/3-11Mechanics-of-MaterialsFall1999/F34792CC-7AA5-47F0-81AD-13664B5F856C/0/frac.pdf.
12. Carpinteri A. *Mechanical Damage and Crack Growth in Concrete*: *Plastic Collapse to Brittle Fracture*. Martinus Nijhoff Publishers: Dordrecht, 1986.



DOI: 10.1002/stc

13. Pollock AA. Some observations on acoustic emission stress time relationships. In *Acoustic Emission and Critical Phenomena*: *From Structural Mechanics to Geophysics*, Carpinteri A, Lacidogna G (eds). Taylor & Francis (CRC Press/Balkema): U.K., 2008.
14. Richter CF. *Elementary Seismology*. Freeman: New York, 1958.
15. Carpinteri A, Lacidogna G, Niccolini G. Critical defect size distributions in concrete structures detected by the acoustic emission technique. *Meccanica* 2008; **43**:349–363.
16. Shiotani T, Fujii K, Aoki T, Amou K. Evaluation of progressive failure using AE sources and improved *b*-value on slope model tests. *Progress in Acoustic Emission* 1994; **7**:529–534.
17. Colombo S, Main IG, Forde MC. Assessing damage of reinforced concrete beam using '*b*-value' analysis of acoustic emission signals. *Journal of Materials in Civil Engineering ASCE* 2003; **15**:280–286.
18. Rao MVMS, Lakshmi KJP. Analysis of *b*-value and improved *b*-value of acoustic emissions accompanying rock fracture. *Current Science* 2005; **89**:1577–1582.
19. Kurz JH, Finck F, Grosse CU, Reinhardt HW. Stress drop and stress redistribution in concrete quantified over time by the *b*-value analysis. *Structural Health Monitoring* 2006; **5**:69–81.
20. Carpinteri A, Lacidogna G, Puzzi S, Niccolini G. Morphological fractal dimension versus power-law exponent in the scaling of damaged media. *International Journal of Damage Mechanics* 2009; **18**:259–282.
21. Lemaitre J, Chaboche JL. *Mechanics of Solid Materials*. Cambridge University Press: Cambridge, 1990.
22. Krajcinovic D. *Damage Mechanics*. Elsevier: Amsterdam, 1996.
23. Cox SJD, Meredith PG. Microcrack formation and material softening in rock measured by monitoring acoustic emission. *International Journal of Rock Mechanis and Mining Science and Geomechanics Abstracts* 1993; **30**:1–21.
24. Turcotte DL. *Fractals and Chaos in Geology and Geophysics*. Cambridge University Press: Cambridge, 1992.
25. Carpinteri A, Lacidogna G, Niccolini G. Fractal analysis of damage detected in concrete structural elements under loading. *Chaos*, *Solitons and Fractals* 2009; **42**:2047–2056.
26. Niccolini G, Durin G, Carpinteri A, Lacidogna G, Manuello A. Crackling noise and universality in fracture systems. *Journal of Statistical Mechanics*: *Theory and Experiment* 2009; DOI: 10.1088/1742-5468/2009/01/P01023.
27. Niccolini G, Bosia F, Carpinteri A, Lacidogna G, Manuello A, Pugno N. Self-similarity of waiting times in fracture systems. *Physical Review E*, *Statistical*, *Nonlinear*, *and Soft Matter Physics*, 2009; **80**:026101-1–026101-6.